Transferable potentials for the Ti–O system

Herman le Roux and Leslie Glasser*†‡

Centre for Molecular Design, Department of Chemistry, University of the Witwatersrand, Johannesburg, WITS 2050, South Africa

Transferable potentials have been derived by computer modelling of the series of higher titanium oxides, from Ti_2O_3 (with Ti^{3+} ions) to TiO_2 (with Ti^{4+} ions), and including the lower members of the series of phases, Ti_nO_{2n-1}, which have mixed oxidation states; some of these are described as crystallographic shear phases. Two potential models have been developed: one comprises coulombic interactions between charge centres, a core–shell model for the oxygen anions, repulsive exponential anion–cation interactions and, in addition, primary antiferromagnetic interactions between Ti^{3+}–Ti^{3+} ions at short distances ($r_{ij} < 2.6$ Å), and secondary repulsive ferromagnetic interactions at longer distances; the second potential differs only in that it uses oxygen anions which are rigid.

The potentials more-or-less successfully model the static crystal structures and their corresponding lattice energies for the full group of oxides included in the modelling, as well as for two independent test structures, and are expected to be equally effective in modelling still higher members of the shear phases, Ti_nO_{2n-1}. Modelling of the dynamic properties (elastic constant and relative permittivity) is not reliable. The shell model oxide potential has a large ('hard') spring constant, and largely mimics the rigid potential, but at the expense of slight instabilities in the modelled structures.

The titanium oxides are a commercially significant group of mineral oxides, with important catalytic, electronic and pigment properties; as a consequence, their structures and the complex phase relations have been extensively studied.[1]

The lowest oxide is TiO. There is a family of higher oxides, Ti_nO_{2n-1}, which are described[2] as having crystallographic shear (CS) structures, and which include the Magnéli phases ($4 \leqslant n \leqslant 9$). The highest oxide is TiO_2, which itself exists in a number of polymorphs: rutile, anatase, brookite, and a number of high-pressure phases, including TiO_2-II as the best characterised.[3,4] To add to this complexity, TiO_2 can accommodate some non-stoichiometry,[5] to form TiO_{2-x}.

Crystals of the Ti–O system may be modelled as essentially ionic structures, but with the possibility of (largely anion) polarisation[6] and electronic interactions.[7] Apart from TiO and its congeners (which we do not consider further), titanium occurs in the oxidation states Ti^{3+} (as in Ti_2O_3) and Ti^{4+} (as in TiO_2). In the intermediate oxides (such as Ti_3O_5), mixtures of the Ti^{3+} and Ti^{4+} oxidation states occur, with the cations generally regarded as disordered. The crystal structures consist of more-or-less regular TiO_6 octahedra which may exhibit corner-, edge- or face-sharing in various combinations, yielding the large variety of crystal structures which is observed.[8] The CS structures consist of rutile-like layers, $(n-4)$ octahedra thick, with corundum-like blocks (Ti_2O_3 has the corundum structure) four octahedra thick between the layers.[9]

There is presently much activity in the derivation of potential functions for computer simulation studies of solid materials.[10] Rutile has often been selected as a material for study[5,11–16] and the difficulties in modelling the structure to yield simultaneously both structural and dynamic properties have been emphasised.[6] Work has also been done on modelling the TiO_2 polymorphs.[17–20]

The structural features of and similarities among the titanium oxides, as mentioned above, have suggested to us the feasibility of developing a simple ion-based, transferable potential which will operate across the Ti–O system, while using the fewest practicable adjustable parameters. The establishment of such a potential is regarded[18] as valuable in modelling any member of the system (except TiO, with its Ti^{2+} ion), especially the complex shear structures of the Magnéli CS phases. No prior attempt to model the full range of structures has been reported.

Cation–cation interactions

Several mineral oxides containing transition-metal cations exhibit physical properties which can be ascribed to interactions between the octahedral site cations.[7] These are of cation–anion–cation nature if cation-occupied octahedra share a common corner. On the other hand, if cation-occupied octahedra have edges or faces in common, interactions may be primarily of a cation–cation nature because of the correspondingly closer approaches. Such cation–cation interactions have been proposed to account for certain magnetic interactions and also for some interesting electrical properties in the Ti–O system.[7]

The strength of such cation–cation interactions is enhanced by the overlap of d-electron wavefunctions at short distances. Such interactions may, therefore, be significant if this dual requirement is met by octahedral site cations with an outer electron configuration $3d^m$ ($m \leqslant 5$) occupying octahedra which share either faces or edges.

In the case of Ti^{4+}, there are no outer d electrons (rutile, for instance, is an insulator) and Ti^{4+}–Ti^{4+} interactions are expected to be small. Ti^{3+}, having a $3d^1$ electron orbital structure, with distorted cation-occupied face-sharing octahedra in corundum-like structures, is expected to exhibit strong short-range Ti^{3+}–Ti^{3+} interactions; indeed, Ti_2O_3 has certain anomalous properties which may be ascribed to such interactions. Hence, special consideration of the Ti^{3+}–Ti^{3+} interaction potential is required in the modelling.

Potential model

Consonant with the above description of the bonding in the titanium oxides, the system has here been modelled as a

† Current address until July 1997: Royal Institution of Great Britain, 21 Albemarle St., London, UK WIX 4BS. E-mail: leslie@ri.ac.uk and glasser@aurum.chem.wits.ac.za

‡ This material was completed and the report prepared by L. Glasser in the absence of Mr. le Roux, owing to the latter's indisposition.

group[21] of integer-charged ionic crystalline solids with Coulombic interactions between the charge centres [eqn. (1)].

$$W_c = \frac{q_i q_j}{4\pi\varepsilon r_{ij}} \quad (1)$$

together with a standard Born–Mayer two-body short-range repulsive potential of the following form between these centres [eqn. (2)].

$$W_r = A_{ij} \exp(-r_{ij}/\rho_{ij}) \quad (2)$$

where ρ_{ij} is a 'softness' parameter.

No van der Waals attractive terms ($-C/r_{ij}^6$) are included in the final models, in common with other work on this system;[5] in fact, an attempt to introduce such a potential resulted in the constant, C, dropping in value towards zero.

For the Ti^{3+}–Ti^{3+} interactions, a pair of interaction potentials has been introduced; one covers the shorter distances to 2.6 Å, while the second acts from 2.9 Å and beyond, with a fitted polynomial spline connecting the potentials over the range from 2.6 to 2.9 Å, to avoid discontinuity in the interaction. The oxygen anions, O^{2-}, have been modelled either as rigid ions or using the Dick and Overhauser shell model.[22] In the latter model,[22,23] the anions are treated as polarisable entities having a charged core containing all the mass, surrounded by a massless spherical shell (which may be displaced from the core), with charge Y supposedly representing the valence electrons. The sum of the shell and core charges constitutes the integral anion charge.

The core and shell are coupled by a harmonic spring, with spring constant k_s. There is, thus, a core–shell potential energy [eqn. (3)]

$$W_{cs} = \tfrac{1}{2} k_s r^2 \quad (3)$$

where r is the relative core–shell displacement in a polarised ion; W_{cs} is zero in the unpolarised condition. An ion polarisibility, α [eqn. (4)], is introduced by this model,

$$\alpha = Y^2/(k_s + f) \quad (4)$$

where f is the sum of forces acting on the shell due to the other ions.

Introducing the shell model increases mathematical flexibility by generating two additional free parameters, Y and k_s, for each class of ion; there is only one kind of oxygen anion in this Ti–O system. The modelling of an observable physical property, the ion polarisibility, thus becomes possible.

Apart from the coulombic terms, only anion shell interactions, *i.e.*, O_s–O_s, between the oxygen anions are modelled[5] in the shell model; core–core interactions between oxygen anions are irrelevant since the repulsion terms are always referred to the shell. Cation–anion interactions are modelled as an interaction between the cation and the anion shell, *i.e.*, Ti^{4+}–O_s and Ti^{3+}–O_s.

Transferable potentials

Transferability of a potential implies that the potential, obtained from the group of crystalline compounds against which it was established, yields satisfactory modelling results for each of the individual crystal structures. It also necessarily implies that potential parameters related to a given ion–ion interaction in a specific crystal structure are likely to be good approximations for a similar ion–ion interaction in a polymorph of the given structure and, in this case, also in a series of related structures.

The establishment of such a potential is *via* optimisation of sets of parameters of ion–ion pair potential equations. The degree of complexity of a transferable potential depends on: (i) the number of possible distinguishable ion–ion interactions which is, by implication, related to the number of different chemical species in a compound formula unit and (ii) the number and kind of structurally related properties which may be included in the fitting, such as elastic constants, relative permittivities, *etc.*

One may legitimately ask how the assumption of transferability of ion–ion interaction potential parameters, as applied above, may be justified in the present situation.

In the particular model chosen, the interactions all depend only on the interionic distance, r_{ij}, corresponding thus to central forces. Since no angular dependence exists, potential parameters established empirically over an averaged ion–ion interaction distance may be expected to be transferable to a different structure with similar average ion–ion interaction distances. Conversely, the presence of different ion species in close proximity to a particular ion–ion interaction may degrade the transferability of the potential parameters from structure to structure.

Evaluation of the individual Ti–O structure models on implementing the established transferable potential does, as we shall see, yield adequate static structure modelling results; the percentage deviation of modelled cell volumes from observed cell volumes proves to be generally $<1\%$ for the TiO_2 structures, 1.1 and 2.6% for the independent test structures (Ti_6O_{11} and γ-Ti_3O_5, respectively), but as large as 14% for low-temperature β-Ti_3O_5, in which there are strong Ti^{3+}–Ti^{3+} interactions. Since other physical properties of the members of the series are largely unknown, dynamic properties have generally not been included in the modelling (except for the elastic constants of rutile), and their values as generated by the model are unlikely to be reliable.

Ti–O system structural properties

Ti^{4+} oxidation state: rutile and other structures

Rutile[24–26] (Fig. 1) has a tetragonal lattice consisting of cations centred in oxygen octahedra. The TiO_6 octahedra share a common edge along the [001] axis and common corners with the other adjacent octahedra, with a cation–anion–cation arrangement of contacts. Although rutile is an insulator, by the addition of small quantities of Ti^{3+}, electrical conductivity can be induced *via* cation–cation or Ti^{3+}–anion–Ti^{4+} interactions.[7] Mean interionic distances[8] in rutile are 1.959 Å for Ti—O, and 2.96 and 3.57 Å for Ti—Ti.

Anatase[27] (Fig. 2) has an elongated tetragonal unit cell with

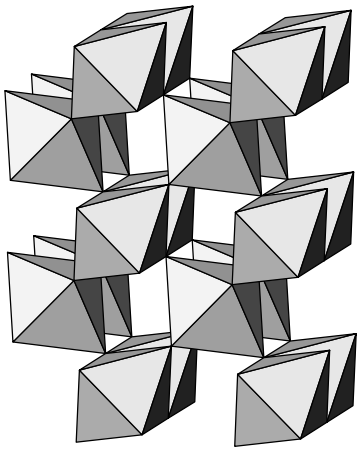

Fig. 1 Packing of TiO_6 octahedra in the tetragonal structure of rutile. The octahedra share edges along the [001] direction, otherwise corners. The *a* axis is vertical along the page in this view. The views in this paper are chosen in an attempt to best display the packing of the octahedra and in a uniform manner; the figures were prepared using ATOMS for Windows, version 3.2 (Shape Software, TN, 1995).

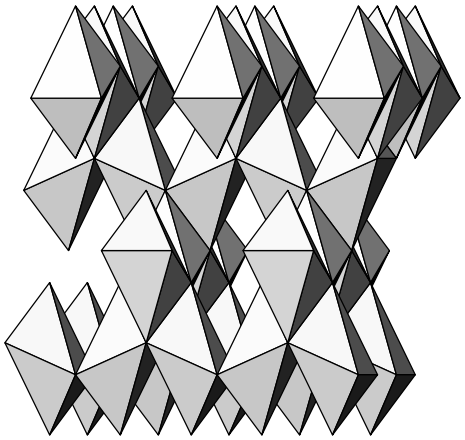

Fig. 2 Packing of TiO_6 octahedra in the elongated tetragonal structure of anatase. The *c* axis is vertical along the page.

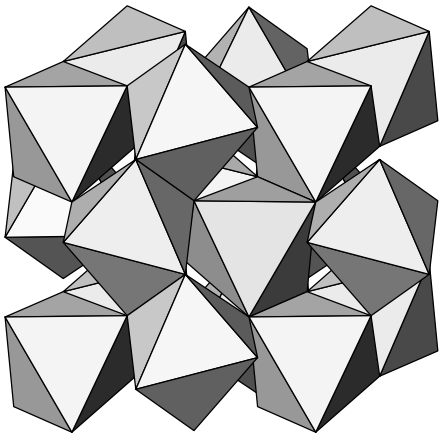

Fig. 3 Packing of TiO_6 octahedra in the orthorhombic structure of brookite. The *c* axis is vertical along the page, and the view is in the [100] direction.

irregular oxygen octahedra, but the Ti—O distances (mean value: 1.917 Å) are nearly equal to each other and to those in rutile. Brookite[28] (Fig. 3) is orthorhombic with a more complex structure, although Ti—O distances are again similar to those in the other polymorphs. The high-pressure phase,[4] TiO_2-II (Fig. 4), has the columbite (α-PbO_2) structure, with TiO_6 octahedra which share two edges; the shared edges have shortened O—O distances.

Ti^{3+} oxidation state: corundum type structure (Ti_2O_3)

Titanium sesquioxide (Ti_2O_3) has a rhombohedral corundum structure[29] (Fig. 5), with a unique threefold axis along which pairs of distorted cation octahedra share faces, occasioning a short cation–cation distance. The octahedra also share common edges with three other octahedra so that short cation–cation distances also occur perpendicular to the unique axis.

Goodenough[7] has suggested that, in the antiferromagnetic structure below the extended transition temperature range (450–600 K), the strong Ti^{3+}–Ti^{3+} interaction leads to direct bond formation between cations. This primary antiferromagnetic interaction occurs between Ti^{3+} cations situated on the trigonal axis, separated by a distance of 2.592 Å, and lying in face-sharing octahedra. A secondary Ti^{3+}–Ti^{3+} cation–cation ferromagnetic interaction, resulting from the octahedral edge-sharing geometry, acts between Ti^{3+} cations 2.990 Å apart and lying in planes separated by 0.322 Å.

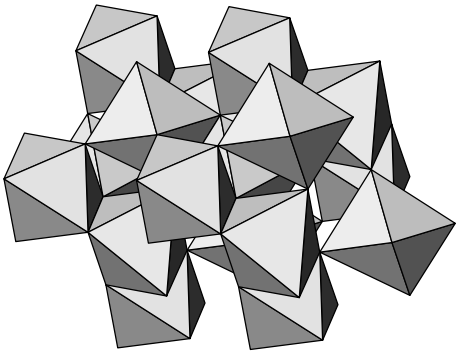

Fig. 4 Packing of TiO_6 octahedra in the orthorhombic structure of the high-pressure phase, TiO_2-II, where the octahedra share two shortened edges. The view is in the [111] direction.

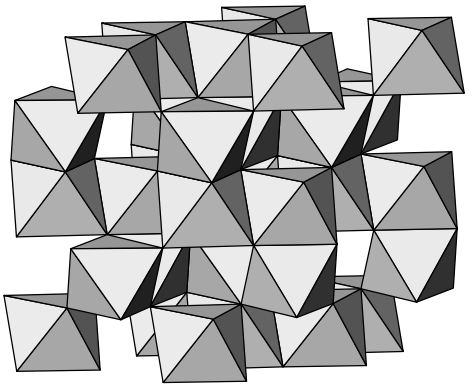

Fig. 5 Packing of TiO_6 octahedra in the rhombohedral corundum structure of Ti_2O_3. The hexagonal *c* axis is vertical along the page. Pairs of octahedra share faces, as seen in the centre, leading to the characteristic short cation–cation distances.

These suppositions on antiferromagnetic bonding interactions are confirmed by recent structural studies[30] of Ti_3O_5 and by structural changes observed[31] in solid solutions of $MgTi_2O_5$–Ti_3O_5, where strong Ti^{3+}–Ti^{3+} interactions bring about a lowering in symmetry from orthorhombic to monoclinic with increasing Ti^{3+} concentration, commencing from $x = 0.72$ in $Mg_{1-x}Ti_{2+x}O_5$.

Mixed Ti^{3+},Ti^{4+} oxidation states: (*a*) trititanium pentoxide (Ti_3O_5)

Trititanium pentoxide (Ti_3O_5) is tetramorphic,[32] with a rapid reversible phase transformation between related high-temperature α- and low-temperature β-phases occurring at approximately 450 K, and for related high-temperature γ- and low-temperature δ-phases at around 236 K; no information is provided[32] on possible interconversions between these two sets of structures. Both the β (or low-Ti_3O_5) and α (or high-Ti_3O_5) modifications of the first pair were modelled in this study. The γ-phase structure was reserved as an independent check of the transferability of the potentials, while the structure of the δ-phase has not been reported.[33]

(i) Low (β)-Ti_3O_5 The low temperature modification, β-Ti_3O_5, has a monoclinic structure[30] (Fig. 6), which may be

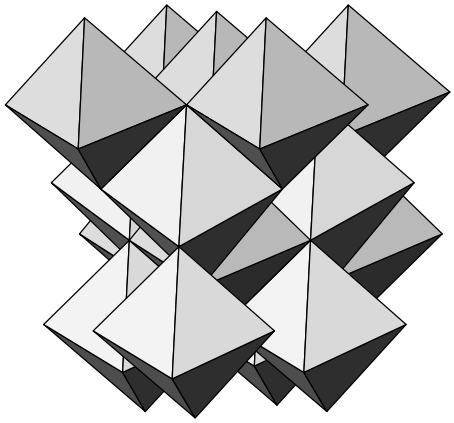

Fig. 6 Packing of TiO_6 octahedra in the monoclinic structure of low (β)-Ti_3O_5, showing sharing of edges by the octahedra. The *c* axis is vertical along the page.

described in terms of distorted TiO_6 octahedra joined by the sharing of edges and corners, thus forming an infinite three-dimensional framework, with five, six or seven shared edges. The extension along the crystallographic *b*-axis is given by octahedra sharing corners.

Ti–Ti interatomic distances of the TiO_6 octahedra joined by corners are throughout of a length not less than 3.8 Å. Ti—Ti distances between edge-sharing octahedra are divided into three different groups, with one very close interaction: (a) 3.17–3.07 Å; (b) 2.82 and 2.77 Å; and (c) 2.61 Å.

The most closely linked Ti^{3+} cations interact across a centre of symmetry, with two electrons available for this bond, since Ti^{3+} has a $3d^1$ outer electron orbital structure, yielding an interaction of primary antiferromagnetic character. Secondary ferromagnetic layer Ti^{3+}–Ti^{3+} interactions are expected between the Ti^{3+} cations at the larger interatomic distances. Ti^{3+}–Ti^{4+} and Ti^{4+}–Ti^{4+} cation–cation interactions, as a consequence of the closed-shell outer orbital electron structure of Ti^{4+}, are expected to be negligible or small, and electron spin–spin coupling between Ti^{3+} and Ti^{4+} is not anticipated.

(ii) High (α)-Ti_3O_5 The high-temperature phase, α-Ti_3O_5, has[30] (Fig. 7) a monoclinically deformed, pseudobrookite-type structure. As opposed to low-Ti_3O_5, all the TiO_6 octahedra of the high-temperature form share six edges with neighbours, with no close cation–cation interactions.

(iii) γ-Ti_3O_5 The third Ti_3O_5 phase, γ-Ti_3O_5 (identified[34] as a member of the Magnéli phases, so extending the range of *n* for these phases to $3 \leqslant n \leqslant 9$), was reserved to test the transferability of the derived potentials. The structure (Fig. 8) is described[34] as containing two independent Ti positions, 'one at and one between the shear planes, each with octahedral O coordination. The two types of octahedra form two different types of infinite chains, one by sharing edges and faces, and one by sharing corners. The chains and their connections are analogous to those found in the two modifications of V_2O_5. There is a partial segregation of Ti^{3+} and Ti^{4+}, and Ti^{4+} concentrates at the shear-plane position.' The shortest Ti—Ti distance is 2.81 Å, suggesting the possibility of some Ti^{3+}–Ti^{3+} cation–cation bonding interaction.

Mixed Ti^{3+},Ti^{4+} oxidation states: (b) Magnéli phases

The room-temperature Magnéli phases[9,35,36] have triclinic structures, described as consisting of a stacking of alternating slabs: a shear-plane slab with fixed geometry, four octahedra thick, with the octahedra sharing three edges or one face and three edges in addition to corners; and a pseudo-rutile slab $(n-4)$ octahedra thick where two edges and corners are shared in a rutile-like fashion. The complex, but regular, arrangements

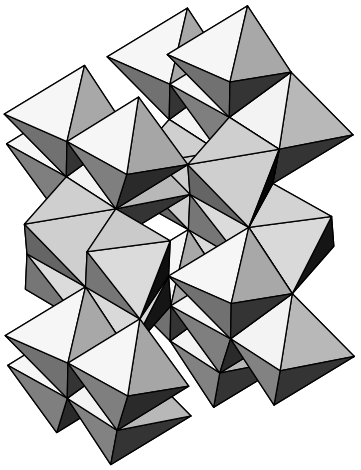

Fig. 8 Packing of TiO_6 octahedra in the monoclinic structure of γ-Ti_3O_5, showing sharing of edges by the octahedra. The *c* axis is vertical along the page.

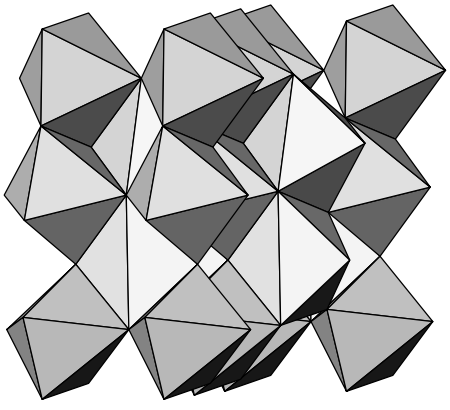

Fig. 7 Packing of TiO_6 octahedra in the monoclinic structure of high (α)-Ti_3O_5, showing sharing of all six edges by the octahedra. The *c* axis is vertical along the page.

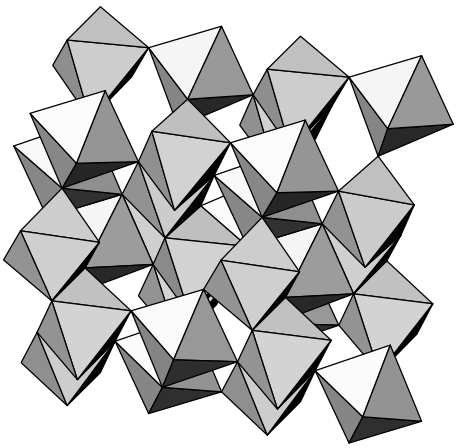

Fig. 9 Packing of TiO_6 octahedra in the triclinic structure of Ti_4O_7. The *c* axis is vertical along the page.

of the octahedra in segmented chains in the various structures are described and depicted in detail in ref. 9 (the structure of the degenerate Ti_4O_7, with no rutile-like slab between the shear-region slabs, is shown in Fig. 9). Ti—Ti distances are 2.81–2.83 Å in the chains within the shear slabs, extending to nearly 3.3 Å at the termini of the chain segments. It would, thus, appear that there is no special Ti—Ti cation bonding to be considered in these CS phases. Ti^{3+}–Ti^{3+} cation–cation interactions of both ferromagnetic and antiferromagnetic nature are found in the low-temperature polymorphs[37] of Ti_4O_7, where there is segregation of the two types of cation; these are, however, not further considered here.

The structure[9] of Ti_6O_{11} was used in this study as an independent check of the quality of fit of the derived potential model for the Magnéli phases.

Crystal packing programs

Modelling of the crystal structures, and optimization of the potential parameters required, was initially performed using Busing's WMIN program,[38] which was programmed with the necessary subroutines in accord with the pairwise interactions described above.

WMIN has the capability of optimizing potential parameters simultaneously across a series of crystal structures, by a least-squares analysis of the deviations of the numerically derived derivatives of the lattice energy against the potential parameters. The so-fitted parameters may then be tested by relaxing the crystal structural constraints, and examining the deviations from the experimental values which result.

At a late stage in this research, Gale's program,[39] GULP, was used in consolidating the results, in allowing for fractional occupancy of the cation sites, and in fitting against the available elastic constants of rutile.

Both of these crystal packing programs are able to generate a list of phonon frequencies and, in addition, GULP will provide a list of elastic constants. It is necessary, for a stable structure, that the phonon frequencies and the leading diagonal of the elastic constant matrix all be positive; the optimised structures in this study were all checked to ensure such stability.

Developing a transferable Ti–O potential

Crystallographic experimental cell data were used to construct the static crystal structures; these data, obtained *via* X-ray powder diffraction techniques, are readily available from the above-referenced literature, and are listed in Table 1.

(i) Modelling the TiO_2 polymorphs: Ti^{4+}–O^{2-} and O^{2-}–O^{2-} interactions

As a point of departure in establishing the short-range interaction potential parameters for a transferable Ti–O potential, the polymorphs of TiO_2 were first evaluated as an independent set in the optimization procedure. Four polymorphs of TiO_2 were modelled: rutile, anatase, brookite, and a high-pressure phase, TiO_2-II. Average O^{2-}—O^{2-} and Ti^{4+}—O^{2-} interionic distances in this set of TiO_2 polymorphic structures are 2.70 and 1.96 Å, respectively. Starting values of potential parameters common to the TiO_2 polymorph set were taken as the literature values established for rutile,[5] including a core–shell model for the oxygen anion. Optimization was accomplished by simultaneous variation of the potential parameters (A and ρ), and the oxygen shell parameters (Y and k_s) and displacements. Nuclear positions and the lattice parameters served as fixed value observables.

Individual potential descriptions were constructed within WMIN for each structure so that observables and the oxygen-ion shell position variations complied with the specific symmetry relations applicable. Potential parameters for the Ti^{4+}–O^{2-} and O^{2-}–O^{2-} interactions, common to the TiO_2 polymorphic set, were thus established.

(ii) Modelling Ti_2O_3: Ti^{3+}–O and Ti^{3+}–Ti^{3+} interactions

The corundum-type structure of titanium sesquioxide (Ti_2O_3) contains Ti ions in the Ti^{3+} oxidation state only. Average interatomic O^{2-}—O^{2-} distances in the Ti_2O_3 structure[24] are 2.80 Å.

By virtue of the close resemblance of the average interatomic O^{2-}—O^{2-} distance in Ti_2O_3 to that of the TiO_2 polymorph set, it was assumed that the set of oxygen parameters obtained *via* optimization in (i) would be transferable to O^{2-}–O^{2-} interactions in the Ti_2O_3 structure model. Ti^{3+}–O^{2-} and Ti^{3+}–Ti^{3+} cation–cation interactions could thus be modelled through optimization, while retaining the transferred values for the O^{2-}–O^{2-} potential parameters.

Two types of Ti^{3+}–Ti^{3+} cation–cation interactions had to be distinguished in establishing the relevant potential parameters. Primary antiferromagnetic Ti^{3+}–Ti^{3+} cation–cation interactions were modelled as acting over interatomic distances <2.6 Å, while secondary ferromagnetic interactions were modelled as acting from 2.9 Å. A fifth-order polynomial spline (with matching energies and first and second derivatives) connected the two regions. Thus, potential parameters A and ρ for antiferromagnetic interactions were obtained for the inter-cationic distance $r_{ij}<2.6$ Å, and secondary ferromagnetic interaction parameters were obtained for $r_{ij}>2.9$ Å. In the event, and after numerous trials, it proved appropriate to choose zero repulsion as representing the antiferromagnetic bonding interaction (*i.e.*, A was finally set to and maintained at zero for this interaction), because this repulsion term tended towards low values in the fitting process. This short distance interaction, then, involves only the cation–cation charge repulsion, with no additional conventional repulsion term, so representing an attractive potential as compared to the other ion–ion interactions.

Owing to the high symmetry of the crystal and the number of variables to be simultaneously varied during the parameter optimization procedure, the requirement for a least-squares analysis, that the total number of observables exceeds the total number of variables, could not be met. In order to generate more flexibility, a complete symmetry release operation was performed. Only the identity operator was retained, and the asymmetric unit was expanded accordingly. The optimization was thus performed in triclinic symmetry, $P1$.

The effect of this symmetry release is to provide a 'feasible set' of solutions from the least-squares analysis since the symmetry is still built into the initial experimental crystal structural data. This 'feasible set' is simply one of a family of related parameters which could, in principle, provide equally valid fits to the experimental data; other such feasible sets will arise from different starting points for the least-squares analysis.

(iii) Modelling Ti_3O_5 and Ti_4O_7: Ti^{3+}–O^{2-}, Ti^{4+}–O^{2-}, Ti^{3+}–Ti^{3+} and O^{2-}–O^{2-} interactions

Average O^{2-}–O^{2-} interatomic distances in the low- and high-Ti_3O_5 structures are calculated as 2.80 Å, while the Ti^{4+}–O^{2-} average interatomic distances amount to 2.00 Å. Transferability of Ti^{4+}–O^{2-} and of O^{2-}–O^{2-} potential parameters, on the grounds of resemblance of the ion situations to those in the TiO_2 polymorph set, was again assumed. Furthermore, average Ti^{3+}–O^{2-} interatomic distances in Ti_2O_3 are calculated as 2.04 Å, which closely resembles those calculated for the low- and high-Ti_3O_5 structures, *viz.*, 2.07 Å, thus permitting transfer of the Ti_2O_3 parameters to these higher oxides.

Primary antiferromagnetic and secondary ferromagnetic cation–cation interactions are then automatically accounted for by virtue of the Ti^{3+}—Ti^{3+} interatomic distances defined by the structure, provided that the assumption is justified of

Table 1 Modelling results for Ti–O compounds[a]

	experimental	flexible oxide potential	rigid oxide potential	δ(%) (exptl.−rigid)
A: TiO_2 polymorphs				
1 rutile	a/Å 4.594	4.580	4.580	−0.30
tetragonal	c/Å 2.959	2.963	2.963	0.15
$P4/2mnm$ (no. 136)	V/Å^3 62.449	62.169	62.169	−0.45
2 anatase	a/Å 3.785	3.779	3.780	−0.15
tetragonal	c/Å 9.514	9.513	9.513	−0.01
$I4/amd$ (no. 141)	V/Å^3 136.300	135.886	135.882	−0.31
3 brookite	a/Å 9.250	9.153	9.153	−1.05
orthorhombic	b/Å 5.460	5.443	5.443	−0.32
$Pbca$ (no. 61)	c/Å 5.160	5.160	5.160	−0.01
	V/Å^3 260.606	257.024	257.025	−1.37
4 TiO_2-II	a/Å 4.515	4.560	4.560	1.00
orthorhombic	b/Å 5.497	5.515	5.515	0.33
$Pbcn$ (no. 60)	c/Å 4.939	4.920	4.920	−0.38
	V/Å^3 122.581	123.756	123.756	0.96
B: Ti_nO_{2n-1} $n=2,3$				
5 Ti_2O_3	a/Å 5.433	5.489	5.489	−0.01
rhombohedral	cos α 0.55092	0.54608	0.54608	
$R\bar{3}c$ (no. 167)	V/Å^3 104.411	108.611	108.611	4.02
Ti_3O_5				
6 low-temp. form (low or β-Ti_3O_5)	a/Å 9.757	12.129	10.459	7.20
monoclinic	b/Å 3.801	3.520	3.484	−8.34
$C2/m$ (no. 12)	c/Å 9.439	9.665	10.923	15.73
	cos β −0.02700	−0.21414	−0.00262	
	V/Å^3 349.901	403.093	398.000	13.75
7 high-temp. form (high or α-Ti_3O_5)	a/Å 9.826	10.448	10.448	6.33
monoclinic	b/Å 3.789	3.486	3.486	−8.01
$C2/m$ (no. 12)	c/Å 9.969	10.920	10.919	9.52
	cos β −0.02195	0.00000	−0.00000	
	V/Å^3 370.026	397.655	397.640	7.15
high-temp. form (γ-Ti_3O_5)	a/Å 10.115	10.396	10.396	2.78
independent example	b/Å 5.075	5.089	5.089	0.29
monoclinic	c/Å 7.181	7.061	7.061	−1.67
$C2/c$ (no. 15)	cos β −0.37500	−0.35404	−0.35404	
	V/Å^3 341.707	349.424	349.424	2.26
C: Ti_nO_{2n-1} $n=4$, …				
8 Ti_4O_7	a/Å 5.600	5.643	5.582	−0.31
triclinic	b/Å 7.133	7.053	7.232	1.40
$P\bar{1}$ (no. 2)	c/Å 12.466	12.796	12.413	−0.43
	cos α −0.08803	−0.03229	−0.07746	
	cos β −0.09011	−0.13469	−0.09078	
	cos γ −0.32078	−0.29174	−0.32408	
	V/Å^3 466.096	481.267	469.113	0.65
Ti_6O_{11}	a/Å 5.552	5.560	5.559	0.13
independent example	b/Å 7.126	7.066	7.061	−0.92
triclinic	c/Å 32.233	33.015	33.089	2.66
$I\bar{1}$ (non-standard)	cos α 0.39169	0.41449	0.41668	
	cos β 0.54347	0.53236	0.53042	
	cos γ −0.31747	−0.30287	−0.30217	
	V/Å^3 716.039	732.933	734.905	2.63

[a]no. refers to space group number, in *International Tables for Crystallography*, ed. T. Hahn, Kluwer, Dordrecht, 3rd revised edn., vol. A, 1992.

transferability of the potential parameters established *via* the Ti_2O_3 structure.

In the Ti_4O_7 shear structure,[36,37] average $O^{2-}—O^{2-}$ interaction distances are calculated as 2.825 Å. $Ti^{4+}—O^{2-}$ and $Ti^{3+}—O^{2-}$ interatomic distances average 2.009 Å and 2.014 Å, respectively. The discrepancies from earlier members of the system are small, and again justify transfer of the potentials.

(iv) The rigid oxide potential

At a late stage in this modelling process, the rigid oxide C2 potential of Collins and Smith[20] became available. This proved to be more successful in obtaining stable TiO_2 crystal structures than was our own flexible ion potential. Thus, we now set up two potentials: the first uses a flexible shell-model oxide ion with the parameters of the Ti^{4+}–O^{2-} C2 potential, but with our core–shell charge distribution and Ti^{3+} parameters; the second uses a rigid oxide ion with the C2 potential and our Ti^{3+} parameters. Attempts at further optimizing the introduced C2 parameters and our core–shell charge distribution in the environment of our full set of eight Ti–O structures did not lead to any substantial changes, even with the computationally expensive 'relax fit' option of GULP,[39] which adjusts the potential parameters to fit the reference structures rather than minimise the internal forces. This suggests that charge distribution is not a very sensitive parameter in the modelling process, which is confirmed by the reliability of the lattice energies relative to the structural parameters (see below).

TiO system modelling results

The optimised parameter values for the two transferable Ti–O potentials, obtained in the manner described above, over the

Table 2 Transferable Ti–O potential models

parameter	optimized values		
	C2 potential of Collins and Smith[20]	flexible oxide potential	rigid oxide potential
$A(Ti^{4+}–O^{2-})$/kJ mol^{-1}	18.02703×10^6	18.02703×10^6	
$\rho(Ti^{4+}–O^{2-})$/Å	0.161170	0.161170	
$A(Ti^{3+}–O^{2-})$/kJ mol^{-1}		0.348357×10^6	
$\rho(Ti^{3+}–O^{2-})$/Å		0.257280	
$A(O^{2-}–O^{2-})$/kJ mol^{-1}	9.189319×10^6	9.189299×10^6	9.189319×10^6
$\rho(O^{2-}–O^{2-})$/Å	0.227815	0.227815	0.227815
k_s/kJ mol^{-1}Å^{-1}		5.20595×10^6	—
Y/e		−2.71547	—
primary antiferromagnetic Ti^{3+}–Ti^{3+} interaction ($r < 2.6$ Å)			
$A(Ti^{3+}–Ti^{3+})$/kJ mol^{-1}		0.0	
$\rho(Ti^{3+}–Ti^{3+})$/Å		—	
fifth-order polynomial		-25.748×10^6	
$(2.6 < r/Å < 2.9)$		$+47.0847 \times 10^6 r$	
		$-34.4078 \times 10^6 r^2$	
		$+12.5599 \times 10^6 r^3$	
		$-2.2901 \times 10^6 r^4$	
		$+166870 r^5$	
secondary ferromagnetic Ti^{3+}–Ti^{3+} interaction ($r \geqslant 2.9$ Å)			
$A(Ti^{3+}–Ti^{3+})$/kJ mol^{-1}		1.71504265×10^6	
$\rho(Ti^{3+}–Ti^{3+})$/Å		0.227815	

range of known structures from TiO_2 to Ti_6O_{11} are listed in Table 2.

These potentials were tested by relaxing the individual static crystal structure models in the Ti–O system, using both WMIN and GULP. Energy minimization within WMIN was accomplished by using the Rosenbrock search technique to adjust structural parameters, and a Newton–Raphson optimiser with BFGS Hessian update[40] in GULP.

The deviations of a fitted structure model from the corresponding experimental crystal structure is conveniently described by the percentage deviations, δ, of the modelled cell constants from the experimental cell values. It must be emphasised that the values of δ need to be judged circumspectly. Individual lattice constant deviations should, as a first approximation, be proportional to each other; so that the geometry of a modelled unit cell fairly accurately describes that of the observed cell. Modelling results for the Ti–O compounds are presented in Table 1. The most striking observation is that the structural results, after relaxing the structures against the potential model, are generally satisfactory except for those structures in which there is significant short-range Ti^{3+}–Ti^{3+} interaction, *viz*., Ti_2O_3 and β-Ti_3O_5. Thus, this interaction has not been adequately modelled, and it appears that some more sophisticated model, such as a polarisible Ti^{3+} core–shell rather than a rigid core alone, and/or an anisotropic oxide ion core–shell, may be required in order to obtain a closer fit. These will require computationally expensive extensions to the modelling.

Cation randomisation

The placement of Ti^{3+} and Ti^{4+} ions in the Ti_3O_5 structures is problematical, and the facility in GULP for assigning fractional occupancy to ion sites was used in a trial-and-error process to select optimal placement of the cations; in fact, satisfactory fitting only occurred when the cations were distributed randomly (*i.e*., each site assigned two-thirds occupancy by Ti^{3+} and one-third by Ti^{4+}) over the possible sites.[31] Also, the initially used early experimental structures of low- and high-Ti_3O_5 did not fit well; by contrast, the more recent results of Grey *et al*.[31] were a substantial improvement.

For Ti_4O_7, there is no significant difference in the results using the flexible ion potential, whether the cations are placed in fixed or in randomised positions;[36,37] on the other hand, the structural fit for the rigid ion potential is substantially degraded (from a volume increase of 0.65% to one of 3.26%) by such randomisation. An equivalently good fit for the volume (−0.51%) is obtained if all the cations are treated as being Ti^{4+} ions having mean charges of $3\frac{1}{2}$; effectively, random positioning with the C2 potential of Collins and Smith.[20] The lattice energy (see below) is, however, poorest in the last case.

For the independent test structure, Ti_6O_{11}, there is little experimental evidence for any ordering in the positioning of the cations, and random placement over the cation sites yields satisfactory fits in the modelling (cell volume error of 2.6%). A better structural fit (volume error of 1.1%) is obtained with an average charge assignment of $3\frac{2}{3}$ to each cation, using the C2 potential as above. The lattice energy is, on the other hand, again poorer using the C2 potential.

Oxygen ion polarisation

Average displacements of oxygen anion shells with respect to the nuclei in the core–shell model of the Ti–O structures, a measure of the extent of polarisation, are very small, given the expectation that the O^{2-} anion is strongly polarised by the

Table 3 Lattice energies per formula unit (kJ mol^{-1}) for the rigid oxide potential

Ti–O series		U_L	U_{rep}	U_L	U_{rep}/U_L(%)
Ti_2O_3		14702[a]	1893	14847	12.75
Ti_3O_5	(β, low-temp.)		3261	27164	12.00
	(α, high-temp.)	24594[a]	3264	27159	12.02
	(γ, high-temp.)		3060	27033	11.32
Ti_4O_7		—	4286	39893	10.74
Ti_6O_{11}		—	6539	64051	10.21
TiO_2	rutile	12150[a]	1128	12493	9.02
	brookite	12149[b]	1128	12462	9.05
	anatase	12147[c]	1140	12454	9.15
	TiO_2-II		1121	12466	8.99

[a]Observed values, from H. D. B. Jenkins, in *Handbook of Chemistry and Physics*, ed. D. R. Lide, CRC Press, Boca Raton, FL, 73rd edn., 1992. [b]Estimated from solution calorimetric data[41] at 971 K. [c]Estimated from solution calorimetric data[41] at 298 K.

Table 4 Lattice energy predictions

Ti–O series	$\langle r\rangle^a$/Å	$-\frac{1}{2}\Sigma n_k z_k^2$	predicted $-U_K$/kJ mol^{-1}	rigid oxide potential $-U_M$/kJ mol^{-1}	difference δ(%)
Ti_2O_3	2.14	15	15 008	14 847	−1.1
Ti_3O_5	2.16	27	27 193		
(β, low-temp.)				27 164	−0.1
(α, high-temp.)				27 159	−0.1
Ti_4O_7	2.16	39	38 409	39 893	3.7
Ti_6O_{11}	2.17	63	59 280	64 051	7.5
TiO_2	2.19	12	12 248		
rutile				12 493	2.0
brookite				12 462	1.7
anatase				12 454	1.7
TiO_2-II				12 466	1.7

$^a\langle r\rangle$ = Weighted mean cation–anion radius sum (using Goldschmidt radii).

highly charged cations; the high value established for k_s in the shell model potential brings about these unexpectedly small oxygen polarisations. This is a clear defect in the model. It has been reported before[6] that simultaneous modelling of the dynamic and structural properties of these materials, so close to ferromagnetic transitions, is exceedingly difficult and is unlikely to be successful with a simple model. We must, therefore, accept this limitation of our simple, structurally biased model in representing the oxygen ion polarisation rather poorly.

Ti–O lattice energies

Energies in these potentials are divided into non-bonded interactions and interactions between bonded atoms. Coulomb electrostatic energy and short-range repulsive energy are included in the non-bonded interaction energy terms. The oxygen anion shell model is modelled analogously to a chemical bond, with the relevant core–shell displacement acting as a bond-stretching term in the energy calculation; however, the oxygen–anion polarisations yield only a very small contribution to the crystal lattice energy due to the tiny core–shell displacements mentioned above.

For convenience and interest, we have divided the total lattice energy, U_L, into a coulomb term and the remaining (repulsive and bond-length displacement) terms, U_{rep}, so that: $U_L = U_c + U_{rep}$.

Calculated Ti–O structure lattice energies per formula unit are presented in Table 3 in sequence of increasing cation oxidation in the structures. The contribution of non-coulombic terms to the total lattice energy is roughly 10%, as is generally observed for ionic crystal systems. The modelled lattice energies within the TiO_2 group are in the expected sequence[20,41] based on the results of solution calorimetry, but the energy differences are much too large.

Ti–O lattice energy predictions *via* a generalised Kapustinskii equation

The empirical Kapustinskii equation for the estimation of lattice energies of ionic solids, applicable to binary ionic materials only, has been generalised[42] to treat ionic solids containing multiple types of ions [eqn. (5)],

$$U/\text{kJ mol}^{-1} = -\frac{1213.9}{\langle r\rangle}\left(1-\frac{\rho}{\langle r\rangle}\right) I \qquad (5)$$

where $\rho = 0.345$ Å, $\langle r\rangle$ is the weighted mean cation–anion radius sum and $I = \Sigma n_k z_k^2$ corresponds to an 'ionic strength' expression.

Table 4 provides a test of our results against the generalised Kapustinskii equation (which is independent of structure). As can be seen, the modelled lattice energies are in excellent agreement with the generalised Kapustinskii equation values. This tends to confirm the transferability from structure to structure of the potentials used, so that any covalency[43,44] between ion types is constant between structures. Lattice energies of ionic systems are quite insensitive to structure (as the relative success of Kapustinskii-type calculations demonstrates).

It was mentioned above that assigning the C2 potential of Collins and Smith[20] to all cations in Ti_4O_7 and Ti_6O_{11} yields improved structural fits but poorer lattice energies; the differences from the Kapustinskii values are 4.4 and 8.7% (*cf.* Table 4 for the rigid-ion potential results), respectively. This conflict suggests some incompatibility of the Ti^{3+} potential among the different environments in which these ions are found.

Summary and recommendation

The group of higher titanium oxides from Ti_2O_3 to TiO_2, and including members of the series Ti_nO_{2n-1}, has been modelled to yield two transferable potentials, which describe the static structures and lattice energies of the series to generally good effect. These potentials do not well represent the antiferromagnetic Ti^{3+}–Ti^{3+} interactions, for which a more elaborate (perhaps anisotropic) potential might be required. Furthermore, the modelled dynamic properties (relative permittivity and elastic constant) are unlikely to be reliable.

It is expected that the transferable potentials here presented will be most useful in structural and lattice energy modelling of other members of the Ti–O series. It is recommended that the rigid ion potential be used in such applications of this force field, since it appears to provide the best balance in calculated properties of these kinds.

The support of Mintek for H. le Roux and for the costs of this project are acknowledged with gratitude. Provision of facilities to L. Glasser by the Royal Institution of Great Britain and by the Chemical Crystallography group at Oxford University, which permitted completion of this work, are also gratefully acknowledged. Particular thanks are offered to Dr J. D. Gale for his support of the work with GULP, and to Dr D. Collins for releasing the unpublished parameters of his C2 potential.

References

1 J. L. Murray and H. A. Wriedt, *Bull. Alloy Phase Diagrams*, 1987, **8**, 148.
2 L. A. Bursill and B. G. Hyde, *Prog. Solid State Chem.,* 1972, **7**, 177.
3 P. Y. Simons and F. Dochille, *Acta Crystallogr.*, 1967, **23**, 334.
4 J. K. Dewhurst and J. E. Lowther, *Phys. Rev. B*, 1996, **54**, R3673.
5 C. R. A. Catlow and R. James, *Proc. R. Soc. London Ser. A*, 1982, **384**, 157; C. R. A. Catlow, C. M. Freeman, S. M. Tomlinson, M. S. Islam, R. A. Jackson and M. Leslie, *Philos. Mag. A,* 1988, **58**, 123.
6 S. M. Tomlinson, C. M. Freeman, C. R. A. Catlow, H. Donnerberg and M. Leslie, *J. Chem. Soc., Faraday Trans.*, 1989, **85**, 367.
7 J. B. Goodenough, *Phys. Rev.*, 1960, **117**, 1442; *Prog. Solid State Chem.*, 1971, **5**, 145.
8 S. Andersson and A. D. Wadsley, *Nature* (*London*), 1966, **211**, 581;

B. G. Hyde and S. Andersson, *Inorganic Crystal Structures*, Wiley-Interscience, New York, 1989.
9 S. Andersson, *Acta Chem. Scand*., 1960, **14**, 1161, 35; Y. Le Page and P. Strobel, *J. Solid State Chem*., 1982, **43**, 314; 1982, **44**, 273.
10 *Philos. Mag. B*, 1996, **73**, Special issue: Interatomic Potentials.
11 C. M. Freeman and C. R. A. Catlow, *J. Chem. Soc., Chem. Commun*., 1992, 89.
12 C. R. A. Catlow, C. M. Freeman and R. L. Royal, 1985, *Physica B,* **131**, 1.
13 C. R. A. Catlow, J. M. Thomas, C. M. Freeman, P. A. Wright and R. G. Bell, *Proc. R. Soc. London Ser. A,* 1993, **442**, 85.
14 V. S. Urusov, L. S. Dubrovinskii, E. A. Vasserman and N. N. Ermin, *Crystallogr. Rep*., 1994, **39**, 391 (Transl. from *Kristallogr*., 1994, **39**, 446).
15 M. Mostoller and J. C. Wang, *Phys. Rev. B*, 1985, **32**, 6778.
16 H. Sawatori, E. Iguchi and R. J. Tilley, *J. Phys. Chem. Solids*, 1982, **43**, 1147.
17 J. E. Post and C. W. Burnham, *Am. Mineral*, 1986, **71**, 142.
18 C. M. Freeman, J. M. Newsam, S. M. Levine and C. R. A. Catlow, *J. Mater. Chem*., 1993, **3**, 531.
19 M. Matsui and M. Akaogi, *Mol. Simul*., 1991, **6**, 239.
20 D. R. Collins and W. Smith, Daresbury Lab. Report, Jan. 8, 1996, ISSN 1362–0207.
21 G. Brink, L. Glasser and R. C. Mboweni, *J. Phys. Chem*., 1989, **93**, 2928; G. Brink, L. Glasser and A. Mattheus, *S. Afr. J. Chem*., 1991, **44**, 125.
22 B. G. Dick and A. W. Overhauser, *Phys. Rev*., 1958, **112**, 90.
23 J. D. Gale, *Philos. Mag. B*, 1996, **73**, 3.
24 S. C. Abrahams and J. L. Bernstein, *J. Chem. Phys.,* 1971, **55**, 3206.
25 W. H. Bauer and A. A. Khan, *Acta Crystallogr., Sect. B*, 1971, **27**, 2133.
26 J. K. Burdett, *Chem. Rev*., 1988, **88**, 3.
27 D. T. Cromer and K. Herrington, *J. Am. Chem. Soc*., 1955, **77**, 4708; *Struct. Rep*., 1955, **19**, 361.
28 E. P. Meagher and G. A. Lager, *Can. Miner*., 1979, **17**, 77; *Struct. Rep. A*, 1979, **45**, 218.
29 C. E. Rice and W. E. Robinson, *Acta Crystallogr., Sect. B*, 1977, **33**, 1342; *Struct. Rep. A*, 1977, **43**, 175. M. G. Vincent, K. Yvon, A. Grüther and J. Ashkenazi, *Acta Crystallogr., Sect. A*, 1980, **36**, 803; *Struct. Rep. A*, 1980, **46**, 397.
30 S. Åsbrink and A. Magnéli, *Acta Crystallogr*., 1959, **12**, 575.
31 I. E. Grey, C. Li and I. C. Madsen, *J. Solid State Chem*., 1994, **113**, 62.
32 S. Åsbrink, L. Gerward and J. S. Olsen, *J. Appl. Crystallogr*., 1989, **22**, 119; S. Åsbrink, *Chem. Scr*., 1988, **28**, 61.
33 S. Åsbrink, personal communication, 1996.
34 S.-H. Hong and S. Åsbrink, *Acta Crystallogr., Sect. B*, 1982, **38**, 2570.
35 M. Marezio and P. D. Dernier, *J. Solid State Chem*., 1971, **3**, 340; M. Marezio, D. B. McWhan, P. D. Dernier and J. P. Remeika, *J. Solid State Chem*., 1973, **6**, 213.
36 Y. le Page and M. Marezio, *J. Solid State Chem*., 1984, **53**, 13.
37 F. Matsushima and E. Iguchi, *J. Phys. Chem. Solids*, 1986, **47**, 45.
38 W. R. Busing, WMIN, ORNL-5747, Oak Ridge National Laboratory revised version, Mar. 1984.
39 J. D. Gale, GULP—General Utility Lattice Program, Imperial College/Royal Institution of Great Britain, version 1.0, 1996.
40 W. H. Press, S. A. Teukolsky, W. T. Vetterling and B. P. Flannery, *Numerical Recipes*, Cambridge University Press, Cambridge, 2nd edn., 1992.
41 A. Navrotsky, J. C. Jamieson and O. J. Kleppa, *Science*, 1967, **158**, 388; A. Navrotsky and O. J. Kleppa, *J. Am. Ceram. Soc*., 1967, **50**, 626; T. Mitsuhashi and O. J. Kleppa, *J. Am. Ceram. Soc*., 1979, **62**, 356.
42 L. Glasser, *Inorg. Chem*., 1995, **34**, 4935.
43 C. Sousa and F. Illas, *Phys. Rev. B*, 1994, **50**, 13974.
44 S. Smart and E. Moore, *Solid State Chemistry*, Chapman and Hall, London, 1992.

Paper 6/07575D; *Received* 7*th November,* 1996